Porous Polylactic Acid–Silica Hybrids: Preparation, Characterization, and Study of Mesenchymal Stem Cell Osteogenic Differentiation

Christos Pandis,* Sara Trujillo, Joana Matos, Sara Madeira, Joaquín Ródenas-Rochina, Sotiria Kripotou, Apostolos Kyritsis, João F. Mano, José Luis Gómez Ribelles

A novel approach to reinforce polymer porous membranes is presented. In the prepared hybrid materials, the inorganic phase of silica is synthesized in-situ and inside the pores of aminolyzed polylactic acid (PLA) membranes by sol-gel reactions using tetraethylorthosilicate (TEOS) and glycidoxypropyltrimethoxysilane (GPTMS) as precursors. The hybrid materials present a porous structure with a silica layer covering the walls of the pores while GPTMS serves also as coupling agent between the organic and inorganic phase. The adjustment of silica precursors ratio allows the modulation of the thermo-mechanical properties. Culture of mesenchymal stem cells on these supports in osteogenic medium shows the expression of characteristic osteoblastic markers and the mineralization of the extracellular matrix.

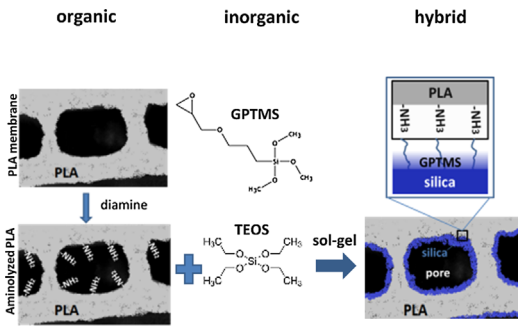

Dr. C. Pandis, Dr. S. Kripotou, Prof. A. Kyritsis
Physics Department, National Technical University of Athens, Zografou Campus, Athens 15780, Greece
E-mail: pandis@mail.ntua.gr
Dr. C. Pandis, S. Trujillo, J. Ródenas-Rochina, Prof. J. L. Gómez Ribelles
Centro de Biomateriales e Ingeniería Tisular, Universitat Politècnica de València, Camino de Vera s/n, Valencia 46022, Spain
J. Matos, S. Madeira, Prof. J. F. Mano
3B's Research Group – Biomaterials, Biodegradables and Biomimetics, University of Minho, Headquarters of the European Institute of Excellence on Tissue Engineering and Regenerative Medicine, AvePark, Taipas, Guimarães 4806-909, Portugal
Prof. J. F. Mano
ICVS/3B's – PT Government Associate Laboratory, Braga/Guimarães, Portugal
Prof. J. L. Gómez Ribelles
Ciber en Bioingeniería, Biomateriales y Nanomedicina (CIBER-BBN), Valencia, Spain

1. Introduction

Poly(lactic acid) (PLA) is a linear aliphatic polyester obtained from renewable resources such as corn starch and sugar.[1] It is a semicrystalline, degradable thermoplastic polymer presenting good biocompatibility and low toxicity.[2] The above characteristics of PLA combined with its good processability have attracted an increasing interest for use in many applications in the biomedical field including scaffolding for bone and cartilage tissue engineering.[3] For many of the above applications, the mechanical properties of pure PLA need to be improved as well as the degradation and biocompatibility characteristics. To that end, the structural unit, lactic acid, is often used for the synthesis of copolymers for example poly(lactide-*co*-glycolide) (PLGA),[4] with tailorable biodegradation while surface modification can improve hydrophilicity and affinity with cells.[5] Among the various physical and chemical

methods, the surface modification using diamines, known as aminolysis, is a very efficient wet chemical route for introducing amino and hydroxyl groups in the surface of polyesters.[6] Furthermore, blending with other polymers[7] or mixing with inorganic particles[8] in order to produce composites appears as an appealing route for tailoring its properties. Various inorganic materials has been used for the production of composites having PLA as the matrix such as nano-hydroxyapatite HAp,[9] layer silicates,[10] carbon nanotubes (CNT),[11] bioglass,[12] or silica nanoparticles.[13,14]

All the above approaches are based on the incorporation of the inorganic phase as a filler in the form of micro or nanoparticles inside the polymer matrix. In this work, a different strategy for the production of hybrid organic–inorganic composite was followed: The inorganic silica phase was synthesized in situ inside the pores of already prepared PLA membranes. To that aim, the versatile method of sol–gel method was employed using TEOS and GPTMS as the silica precursors. The sol–gel reactions were performed in acidic conditions in order to produce a continuous silica phase covering the pore walls of the membranes.[15,16] The silica network was produced after the hydrolysis and condensation of TEOS and GPTMS. The latter also has an epoxy ring to one end permitting to link with functionalized PLA and thus can serve as coupling agent between the silica and the PLA phase. In order to enhance the affinity with PLA, its surface was functionalized by introducing amino groups. The hypothesis is that GPTMS can act as a bridge between the silica network and the aminolyzed PLA through the reaction of the epoxy ring with the free amino groups introduced in the polymer. Porous membranes with various TEOS/GPTMS ratios were fabricated and the steps of the preparation procedure were assessed by various techniques. The morphology, water sorption behavior, thermal, and mechanical properties of the prepared hybrid membranes were studied and discussed. Culture of mesenchymal stem cells on these supports in osteogenic medium shows the expression of characteristic osteoblastic markers and the mineralization of the extracellular matrix. Furthermore, the proliferation and osteoblastic differentiation potential was studied using porcine bone marrow mesenchymal stem cells.

2. Experimental Section

2.1. PLA Membranes Preparation and Functionalization

PLA porous membranes were prepared by the freeze extraction method:[17] PLA (Natureworks Ingeo 4042D) was dissolved in dioxane (99%, Scharlau) to prepare a solution of 10% w/w. After stirring for 24 h, the solution was poured in Teflon molds, frozen with liquid nitrogen and put at −20 °C. Already frozen ethanol at −20 °C was used to fully cover the membranes and being changed for at least three times during 48 h in order to remove the solvent. The membranes were left at room temperature for 24 h and vacuum dried at 40 °C for 24 h before further treatment. Furthermore, PLA films were prepared by solvent casting.

The introduction of amino groups in the surface of already prepared PLA films and membranes was performed by an aminolysis reaction using 1,6-hexanediamine (Acros Organics). Preliminary tests varying reaction time, temperature, and concentration were performed and finally a mild procedure described in ref.[18] was chosen: the membranes were immersed in a solution of 1,6-hexanediamine in isopropanol (Scharlau) with a concentration of 10 mg ml^{-1} at 58 °C for 1 min 30 s. In order to remove any unreacted species, the membranes were rinsed with distilled water and left in a solution of isopropanol/water 1:1 for 24 h changing it two times. Finally, the aminolyzed membranes were vacuum dried at 40 °C for 24 h.

2.2. Introduction of Silica Phase Inside the Membrane Pores

Sol–gel method was used for the introduction of the silica phase inside the pores of the already prepared membranes. Silica precursor was a mixture of tetraethyl orthosilicate (TEOS) (Sigma–Aldrich) and 3-glycidoxypropyltrimethoxysilane (GPTMS) (Sigma–Aldrich). The molar ratio of GPTMS with respect to TEOS in the sol–gel solution was varied between 0.05 to 1, while the molar ratios of the rest components, with respect to TEOS as well, (water, ethanol, and chloride acid) of the starting solution were kept constant (1, 2, and 0.0185, respectively). After 1 h of stirring, the above solution was transferred to a glass tube allowing to fully cover the PLA membranes. In order to assure that the pores of the polymer be filled by the prepared solution, a vacuum pump attached to the reaction tube was used prior to the introduction of the solution. After 15 min, the samples were removed from the solution, and superficially rinsed with water:ethanol 2:1 v/v solution. The membranes were left at room temperature for 24 h and then heated to 90 °C for 24 h. Finally, the samples after the completion of sol–gel reactions were washed with distilled water to remove any unreacted species.

2.3. Morphology Characterization

The morphology of the PLA and PLA/silica membranes was studied by means of scanning electron microscopy (SEM) in a JSM-6300 microscope (JEOL) using an accelerating voltage of 10 kV with the samples previously sputter coated with gold. The cross-section visualization of the samples was done after being cryofractured using liquid nitrogen.

Porosity was measured by a gravimetric method. Firstly, the dried samples were weighed before and after being immersed in ethanol. Porosity, p (%), was calculated as the quotient of the volume of pores (V_{pore}) and the total volume of the membrane (V_{total}).

The volume occupied by pores, V_{pores}, was deduced from the weight difference between dry (m_{dry}) and wet (m_{wet}) sample,

$$p(\%) = \frac{V_{pores}}{V_{Total}} = \frac{V_{pores}}{V_{polym} + V_{pores}} \times 100 \quad (1)$$

Macromol. Biosci. 2014, DOI: 10.1002/mabi.201400339

The volume of the polymer, V_{polym}, and of the pores, V_{pores}, was calculated using the density of ethanol ($\rho_{ethanol} = 0.79\ g\ cm^{-3}$) and of PLA ($\rho_{PLA} = 1.25\ g\ cm^{-1}$).

2.4. Gel Permeation Chromatography (GPC) and Fourier Transform IR Analysis

Molecular weight distribution for membranes of different aminolysis time was studied using a chromatograph Waters 1525 fitted with a Binary HPLC pump, Waters® 2414 refractive index detector and four serial columns Styragel HR 5 THF, Styragel HR 4 THF, Styragel 1 THF, Styragel HR 0.5 THF, using tetrahydrofuran (THF) as mobile phase. The flow rate was 1.0 ml min^{-1} and the samples were prepared with 5% w/v in THF. The concept of universal calibration was used to estimate the molecular weight of pure PLA and PLA aminolyzed using monodisperse polystyrene (PS) standards SM-105 (Showa Denko) according to the procedure reported in ref.,[19] using $K_{PLA} = 5.45 \times 10^{-5}$ dL g^{-1} and $a_{PLA} = 0.73$ as the Mark–Houwink–Sakurada parameters for PLA[20] and $K_{PS} = 1.14 \times 10^{-4}$ dL g^{-1} and $a_{PS} = 0.716$ for PS. More details on the calculation procedure could be found in ref.[21]

Fourier-transform infrared (FTIR) spectra were collected in a Thermo Nicolet Nexus FTIR spectrometer (Thermo Fischer Scientific, Inc., Waltham, MA, USA), in the attenuated total reflection mode (ATR). The spectra resulted from averages of 128 scans at 4 cm^{-1} resolution, between 650 and 4 000 cm^{-1}.

2.5. Thermomechanical Characterization

The thermal properties of samples were studied by thermogravimetric analysis (TGA) using a SDT-Q600 (TA-Instruments) equipment in nitrogen atmosphere with a constant heating rate of 10 °C min^{-1} from room temperature to 650 °C.

Differential scanning calorimetry (DSC) measurements were performed using a Pyris 1 apparatus (Mettler Toledo). In order to erase the effects of any previous thermal history, the samples were heated to 180 °C and then subjected to a cooling scan down to 0 °C at 20 °C min^{-1}, followed by a heating scan up to 180 °C at a rate of 10 °C min^{-1}.

2.6. Water Vapor Sorption

Water vapor adsorption experiments were performed using a VTI-SA+ (TA Instruments) vapor sorption analyzer at 25 °C. The equilibrium water vapor sorption isotherms were obtained for water activities up to 0.95.

2.7. Cell Culture Studies

2.7.1. Cell Harvesting and Subculturing

Primary cell culture mesenchymal stem cells was obtained from pig bone marrow. Femur from four-month-old porcine donor was fleshless, disinfected with 70% ethanol and sawn the femora upper part. Gelatinous bone marrow was removed from medullary cavity washed with culture medium (Dulbecco's modified Eagle's medium (DMEM; 10938025, Fisher), 1% Pen/Strp ((10000 units ml^{-1} penicillin, 10000 μg ml^{-1} streptomycine), D17-602E, Lonza), 10% fetal bovine serum HyClone (FBS, SH30071.03, Fisher), and 10% GlutaMAX (61965, Gibco)) and triturated with a syringe with 16-gauge needle. Sample was homogenized, centrifuged at 650*g* for 5 min and supernatant was discarded. Sample was resuspended and centrifuged again before to filter using a 40 μm nylon filter. Finally, cells were seeded in T75 flasks at a density of 10×10^6 cells/flask. Bone marrow mesenchymal stem cells (BM-MSCs) were expanded until passage 2 using *expansion medium (Xpan)* (DMEM, 1% Pen/Strp, 10% FBS, 10% GlutaMAX, 5 ng ml^{-1} fibroblast growth factor-2 (FGF-2, PCYT-218, Eurobio) in 75 cm^2 cell culture flasks at 37 °C, 5% CO_2 and 95% humidity.

Mycoplasma test (MycoAlert™ Plus Mycoplasma Detection Kit, Lonza) was performed before each culture according to the manufacturer's guideline. Briefly, 1.5 ml of 24 h culture supernatant was centrifuged and 100 μl were transfer into a 96-well-plate. Then, 100 μl of MycoAlert™ Plus Reagent were added and incubated 5 min at RT, samples were read (reading A). Finally, 100 μl of MycoAlert™ Plus Substrate were added to each sample, incubated for 10 min at RT and samples were read (reading B). Ratio of reading B/reading A was calculated. Ratios below 1 were negative for mycoplasma.

2.7.2. Differentiation Study

Differentiation study culture was performed in 5 mm diameter samples at 1, 7, 14, and 21 d. Samples sterilized with gamma ray radiation (25 kGy performed by Aragogamma) were washed in Dulbecco's phosphate buffer saline (DPBS; D5652 Sigma) and incubated with Xpan medium for 1 h at 37 °C, 5% CO_2 and 95% humidity. Samples were deposited in 3% agarose coated 96-multiwell plate seeded at a density of 51 000 cells cm^{-2} in Xpan medium. After 24 h of cell seeding, culture medium was changed with *osteogenic differentiation medium* (DMEM; 1% Pen/Strp, 10% FBS, 0.31×10^{-5} M dexamethasone (D2915 Sigma), 0.05 mM ascorbic acid (A4403 Sigma) and 1 M β-glycerol phosphate (50020 Sigma)). Samples were previously conditioned in DMEM for 24 h at 37 °C, 5% CO_2 and 95% humidity.

2.7.3. DNA and Collagen Measurement

Samples were removed at 1, 7, 14, and 21 d and washed with DPBS and stored at −80 °C until the analysis was performed. After thawing, cells were digested adding papain (Sigma) at 161 μg ml^{-1} dissolved in *activation buffer* (63 mg of L-cysteine hydrochloride hydrate (c7477, Sigma) in 40 ml of *papain buffer extraction* (PBE; 100 ml miliQ water, 0.653 g Na_2HPO_4 (S3264, Sigma), 0.648 g NaH_2PO_4 (S3139, Sigma), 1 ml of ethylenediaminetetraacetic acid 500 mM (EDTA; 15575020, Invitrogen), pH 6.5)) to solubilize the biomolecules and protect it from enzymes released from lysed cells. Samples were incubated for 18 h at 60 °C in the hotbox at 10 rpm. Digested samples were used immediately for DNA quantification assays, and they were stored at −80 °C until collagen quantification assay.

DNA content was performed with Quant-iT™ PicoGreen® dsDNA Kit (Invitrogen) according to the manufacturer's guideline. Briefly, 28.7 μl of digested samples and standards were placed into black 96-well-plate, 71.3 μl of Picogreen Solution 1:200 in TE buffer

and 100 μl of 1× Tris–EDTA buffer (TE). Samples were incubated 5 min minimal light conditions. Samples were read in a Victor3 microplate reader (Perkin Elmer) at 480 nm excitation and 520 nm emission. Standard curve was constructed using a commercial digested DNA.

Total collagen quantification was performed by means of hydroxylation of hydroxyproline.[22,23] Digested sample at 7, 14, and 21 d was mixed with the same volume of 37% HCl and incubated for 18 h at 110 °C. Samples were cooled centrifuged at 5 000*g* for 5 min. Then, samples were dried at 45 °C for 2–3 d and were resuspended in 200 μl of miliQ water. Samples were centrifuged and supernatant was immediately analyzed. Assays were performed in 96-well-plates adding 60 μl in triplicate of each sample and control, 20 μl of *assay buffer* (1.5 ml *n*-propanol (402893, Sigma), 1 ml miliQ water, 5 ml *citrate stock buffer* (80 ml miliQ water, 5.04 g citric acid monohydrated (c1909, Sigma), 11.98 g sodium acetate trihydrate (S7670, Sigma), 7.22 g anhydrous sodium acetate (S2889, Sigma), 3.2 g NaOH (655104, Sigma), 1.26 ml glacial acetic acid (695084, Sigma), pH 6.1)) and 40 μl of *Chloramine-T reagent* (141 mg Chloramine-T (857319, Sigma), 500 μl miliQ water, 500 μl *n*-propanol, 4 ml *citrate stock buffer*). Plates were covered with tinfoil and incubated for 20 min at RT to allow hydroxyproline oxidation to complete. Then, 80 μl of *DMBA reagent* (6 ml *n*-propanol, 3 ml 70% perchloric acid (244252, Sigma), 4.5 g 4-(dimethylamino)benzaldehyde (39070, Sigma)) was added. Plates were covered with sealplate film and incubated at 60 °C for 20 min. After cooling, plates were read at 570 nm in a plate spectrophotometer VICTOR3 from Perkin Elmer. Standard curve of known concentrations of 50 μg ml^{-1} of *cis*-4-hydroxyproline (56246, Sigma) in *PBE* stock solution was used.

2.7.4. Alkaline Phosphatase Activity Quantification

The ALP activity was measured as the conversion of *p*-nitrophenylphosphate into *p*-nitrophenol. Samples of 21 d were placed on eppendorfs with 100 μl of lysis buffer (2% Triton X-100 (T9284 Sigma), 10 mM Tris–HCl ($C_4H_{11}NO_3 \cdot HCl$, 93314 Sigma), pH 7.2) and incubated 10 min on ice and finally sonicated for 2 min. After that, samples were centrifuged and supernatants were added into new eppendorfs. Supernatants were incubated for 2 h at 37 °C with *p*-nitrophenylphosphate (1 mg ml^{-1} (71770 Fluka) dissolved in *substrate buffer* (50 mM glycine, 1mM $MgCl_2{\cdot}(H_2O)_6$, pH 10.5)) on minimal light conditions and the reaction was stopped with 50 μl NaOH 1 M. One hundred microliters of each sample was added in triplicate into a 96-well-plate and were read at 405 nm with a plate spectrophotometer (VICTOR3, Perkin Elmer). Dilutions of *p*-nitrophenol (N7660 Sigma) in NaOH 0.02 M at various known concentrations were used to construct the standard curve.

2.7.5. Histochemical Staining

Alizarin red staining was assessed to detect calcium precipitates. Briefly, samples were washed with DPBS and then they were immersed in chilled absolute ethanol for 10 min at RT. After that, samples were rinsed with DPBS and then with water. *Alizarin RedS solution* (1% Alizarin RedS (A5533, Sigma) in water, pH 4.1) was added for 1 min at RT and finally, samples were washed gently with water and the staining was fixed with absolute ethanol.

Picrosirius red staining was performed to detect collagen upon samples. Briefly, samples were washed with distilled water for 10 min and then they were immersed in *Pricrosirius red solution* (0.5 g Direct Red 80 (365548, Sigma) in 500 ml of saturated aqueous solution of picric acid) for 25 s. Then samples were immersed in 0.5% acetic acid solution for 30 s and distilled water for 30 s. Finally, a counterstaining with hematoxylin for 30 s washing with water was performed. Samples were mounted with 85% glycerol in water.

3. Results and Discussion

3.1. Aminolysis of PLA Membranes

The first step of the preparation procedure was the fabrication of porous PLA membranes and their functionalization with free amino groups in order to be able to react later with GPTMS. A diamine, 1,6-hexanediamine, was used for that purpose as has been proposed by other authors.[18,24] The concentration of the diamine, the temperature, and the time of the aminolysis reaction influence the final concentration of the amino groups in the functionalized surfaces. As it is well known for such reactions in polyesters, the aminolysis involves the chain scission of the polymer backbone that leads to lowering of the molecular weight and degradation. So there is a trade-off between the degree of aminolysis and the downgrade of mechanical properties. Thus, it was critical to choose the optimal conditions to perform the aminolysis reactions and to introduce free amino groups without significant expense on the mechanical properties. To that end, a preliminary assay was conducted in order to choose the parameters of the aminolysis reaction and specifically the reaction time. The concentration of the diamine solution was kept constant and the temperature of the process was fixed at 58 °C in order to study the influence of the reaction time. The reaction time was 90, 900, and 9 000 s. Longer times led to significant weight loss, degradation of PLA, and severe reduction of the mechanical properties. FTIR was used as a tool to assess the efficiency of the aminolysis reaction on the introduction of amino groups and gel permeation chromatography (GPC) was performed to evaluate the molecular weight distribution after the reaction. The results in terms of $\overline{M}_w$ and $\overline{M}_n$ and polydispersity index (PDI) obtained from GPC are reported in Table 1. The reduction of $\overline{M}_w$ with aminolysis time was confirmed and a significant increase of PDI for the reaction performed at 90 s is observed. In that way, a milder condition was chosen for the functionalization of the PLA membranes through aminolysis reactions at 58 °C for 90 s.

In Figure 1, the ATR-FTIR spectra of pure PLA, aminolyzed PLA (amPLA) and amPLA + TEOS/GPTMS 1:1 are presented. The characteristic bands of PLA structure could be identified in the obtained spectrum of pure PLA film:[25,26] The —C═O carbonyl stretch at 1 748 cm^{-1}, the —CH_3 bend at 1 452

Table 1. $\overline{M}_w$ $\overline{M}_n$ and polydispersity index (PDI) obtained from GPC for aminolyzed PLA for various times.

	GPC		
Aminolysis time [s]	$\overline{M}_w$	M_v	**PDI**
0	340 000	210 000	1.62
90	240 000	70 000	3.43
900	130 000	70 000	1.81
9 000	44 000	25 000	1.74

cm^{-1}, the —CH— deformation at 1 380 and 1 359 cm^{-1}, the —C—O— stretch at 1 180, 1 128, and 1 078 cm^{-1} while the band appearing at 871 and 756 cm^{-1}, can be attributed to the amorphous and crystalline phases of PLA, respectively. Apart from those characteristic bands, the spectrum of the amPLA film presents two additional peaks located at 1 648 and 1 548 cm^{-1}. The latter peaks correspond to amide I and amide II bands, respectively, and are used as a confirmation of the presence of amino groups in aminolyzed polyesters.[27,28] Thus, the appearance of the above bands provides a clear proof of the introduction of amino groups on the surface of PLA by the reaction employed using diamine. Furthermore, the decrease of amide I in the spectrum of PLA + TEOS/GPTMS 1:1 implies that the functional groups are consumed providing an indication that the introduced amino groups have reacted with the epoxy groups of GPTMS.

3.2. Morphology

The morphology of the cross-section of the membranes was studied by SEM. Representative micrographs are presented in Figure 2 showing the interconnected porous structure of the membranes with a pore size around 10 μm. The porosity of the initial PLA membranes is dictated by the conditions selected for the freeze-extraction, namely the concentration of PLA in dioxane and the protocol followed for the freezing of PLA/dioxane solution.[29] The above parameters provide a versatile tool for adjusting the pore size and the overall porosity of the prepared membranes. In the present study, a concentration of 10% PLA in dioxane and the rapid freezing with liquid nitrogen yielded the porous structure shown on SEM micrographs with a porosity of 77% as evaluated by gravimetric techniques. It is worth noting that the combination of complementary techniques (e.g., particle leaching) could lead to structures characterized by macroporosity giving a high versatility for the control of pore architecture to meet the needs of the application envisaged.

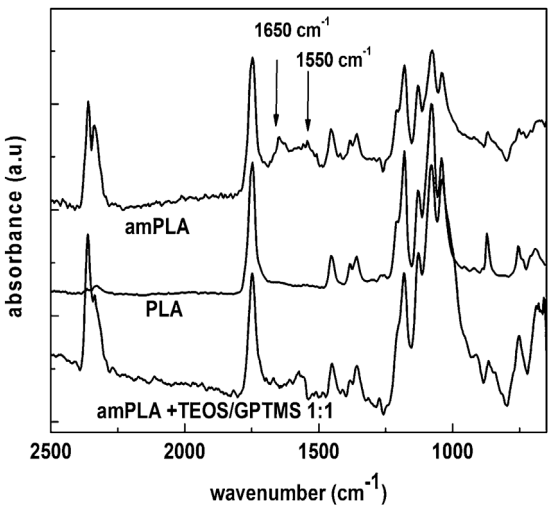

Figure 1. FTIR spectra of pure PLA, amPLA, and amPLA + TEOS/GPTMS 1:1.

The membranes after the functionalization with amino groups show the same morphology compared to unfunctionalized membranes (Figure 2a,b). The above structure of well-interconnected pores is retained also after the completion of sol–gel reactions inside the pores of the membranes. The porosity of the scaffolds is reduced in the hybrid membranes after performing the sol–gel reactions, as expected. The porosity obtained varies between 66 and 75% depending on the ratio of the silica precursors TEOS/GPTMS and is reported in Table 2. The lower porosity of 66% is obtained when only TEOS is used as the precursor of the silica phase.

The acidic conditions used for performing the sol–gel reactions resulted in the formation of continuous silica phase covering the walls of PLA pores. It is well established that low pH values lead to continuous silica phase while basic conditions yield to the synthesis of microparticles and more branched species.[30,31] The proposed morphology is proved by the SEM micrographs showing the residue after pyrolysis at 850 °C (Figure 2f). It should be noted that no residue was observed after pyrolysis of pure PLA and amPLA membranes. The above observation combined with the SEM analysis of the residues of hybrid materials after pyrolysis provide an indirect but convenient way to study the structure of the inorganic component. After pyrolysis, the organic phase is removed and only the inorganic component of the hybrid materials is left revealing the structure of the inorganic phase composed of silica. The hypothesis of the preparation of a two co-continuous phase composite with a high porosity is clearly evidenced from the above analysis.

3.3. Thermogravimetric Analysis

The TGA thermograms and the corresponding derivative curves of pure PLA, amPLA, amPLA + TEOS, and amPLA +

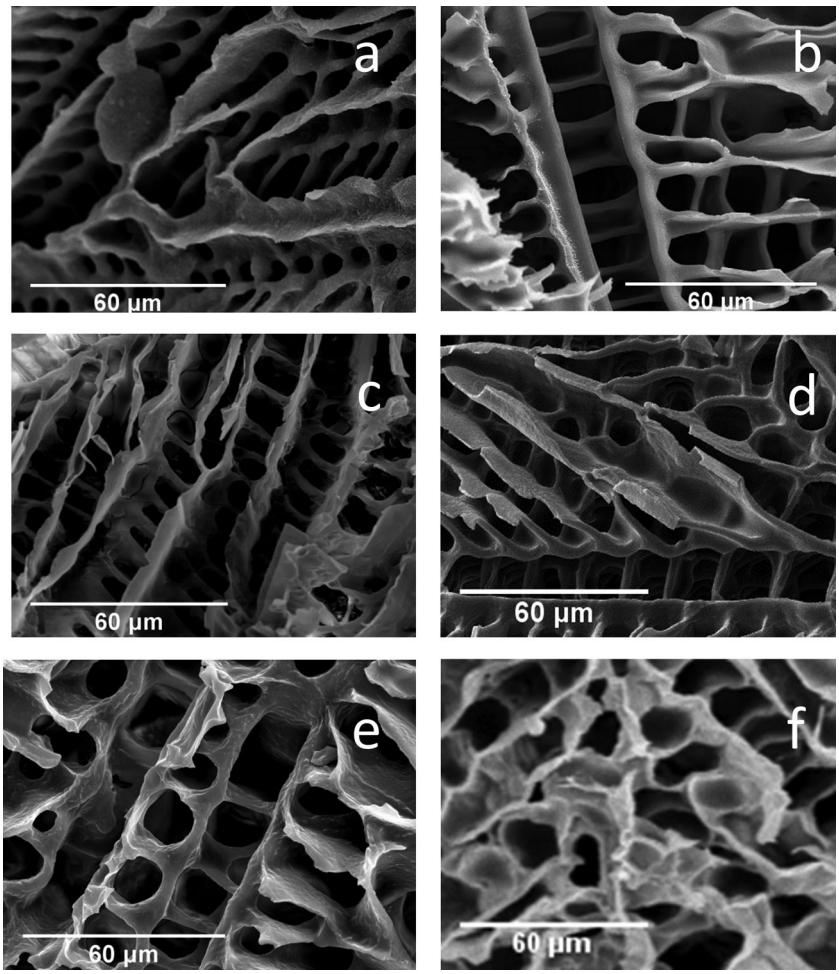

Figure 2. SEM micrographs; a) pure PLA, b) amPLA, c) amPLA + TEOS/GPTMS 1:0.1, d) amPLA + TEOS/GPTMS 1:0.5, e) amPLA + TEOS/GPTMS 1:1, and f) pyrolysis residue of amPLA + TEOS/GPTMS 1:0.5.

Table 2. Porosity of the membranes and residue after pyrolysis at 850 °C.

Sample	Porosity [%]	Residue after pyrolysis [%]
amPLA	77	–
amPLA + TEOS	66	26
amPLA + TEOS/GPTMS 1:0.05	70	16
amPLA + TEOS/GPTMS 1:0.1	75	14
amPLA + TEOS/GPTMS 1:0.2	68	16
amPLA + TEOS/GPTMS 1:0.5	67	12
amPLA + TEOS/GPTMS 1:1	68	14

TEOS/GPTMS membranes prepared with various TEOS/GPTMS ratios are presented in Figure 3. An initial weight loss at around 100 °C could be seen only for the PLA + TEOS membrane. The above weight loss is associated with the evaporation of water bound or trapped in the membranes. It is well known that PLA is a highly hydrophobic polymer as will be seen later in the discussion of water sorption measurements. Silica presents a hydrophilic character due to the remaining silanol groups (Si—OH), which are always present in its surface. Previous studies have shown that the binding sites of silica prepared by sol–gel are already occupied by water molecules at a relative humidity level of 20% with a water content around 10%.[32]

By increasing the temperature, the thermal degradation of the organic part takes place. Pristine PLA and amPLA present similar profiles of one step degradation within a narrow temperature range, which is depicted by only one peak in the DTA signal located around 350 °C. The onset decomposition temperature (T_d) of aminolyzed PLA is slightly lower compared to pure PLA that could be justified by the slight decrease of molecular weight[33] upon aminolysis as shown earlier. The decomposition temperature of the composites shifts to higher temperatures except for the amPLA + TEOS/GPTMS 1:1 membrane. The profile of the samples containing silica presents also one step degradation apart from the amPLA TEOS/GPTMS 1:1 membrane, which shows two peaks at 328 and at 400 °C. Interestingly, the peak at higher temperature is shifted to lower temperatures compared to the one that correspond to TEOS/GPTMS 1:1 as shown in Figure 3c.

3.4. Thermal Properties

Figure 4 shows the DSC thermograms of the membranes recorded during the first and second heating scan with a heating rate of 10 °C. Pure PLA and amPLA present only the endothermic peak corresponding to the melting of PLA while the glass transition is barely observable. The same behavior holds also for the composites with silica expect for the one where silica was produced using only TEOS. The melting peak recorded is attributed to the formation of crystallites during the step of the preparation procedure where the samples stayed at 90 °C for 24 h. The above conditions served as an annealing process allowing the formation of crystallites.

Macromolecular Journals

Macromol. Biosci. **2014,** DOI: 10.1002/mabi.201400339

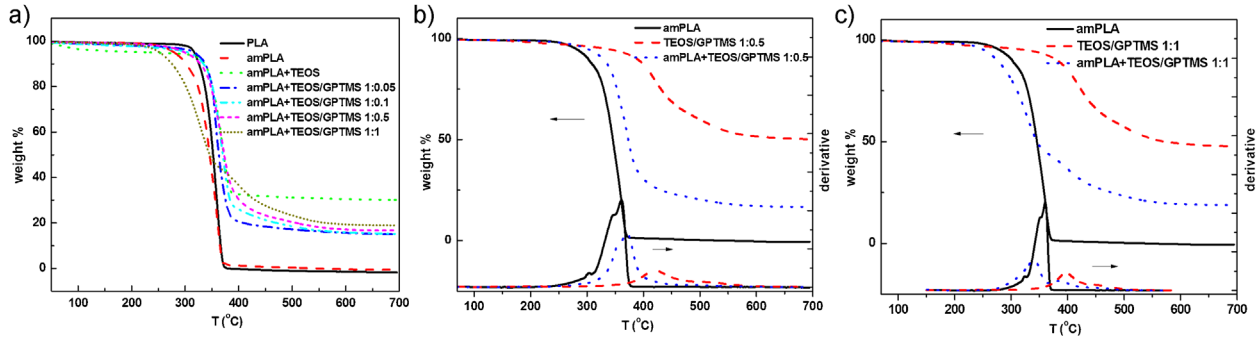

Figure 3. TGA thermograms of PLA, amPLA, and amPLA + TEOS/GPTMS.

The glass transition temperature (T_g), the melting temperature (T_m), and the increment of the heat capacity (ΔC_p) at glass transition of the various samples are also reported in Table 3. It is noted that all the values of ΔC_p presented are normalized to the amorphous part of the samples by taking into account the organic part and the crystalline fraction of PLA. The crystalline fraction, x_c, was estimated by using the relation $x_c = \Delta H/\Delta H_o$, where ΔH is the measured enthalpy of fusion of the sample and ΔH_o is the enthalpy of fusion of the completely crystalline material. Taking into account the ΔH of 100% of PLA as 93.1 J g^{-1},[34] the values of x_c were calculated and reported in Table 3.

The thermograms corresponding to the second heating scan and after erasing the thermal history present different thermal characteristics. It has been shown in previous works that the formation of crystallites in PLA is strongly dependent on the cooling rate used after the melting and that cooling rates higher than 5 °C lead to an amorphous material.[34,35] After using a cooling rate of 10 °C in the present case a clear glass transition is observed for all the samples in the second heating scan while the parameters calculated from the analysis are reported in Table 3. The T_g of PLA remains unaffected and around 60 °C apart from the amPLA TEOS/GPTMS 1:1, which presents a broader glass transition with a T_g at 48 °C. Additionally, all the samples except for PLA and PLA + TEOS present an exothermic peak during heating, the so-called cold crystallization and its characteristic temperature (T_{cc}) is reported in Table 3. As temperature increases, the crystallites formed during the latter process are melted to give the recorded melting peak. The different behavior between the composite with only TEOS and those that incorporate GPTMS probes the influence of the latter on the segmental dynamics of PLA. Interestingly there is a trend of lowering of the cold crystallization temperature upon increasing the GPTMS content.

Moreover, from the data presented in Figure 4, the integration of the DSC trace covering both crystallization and melting peaks gives a negligible enthalpy, characteristic of a nearly amorphous material[34] as can been seen in Table 3. Another alteration in the melting of PLA is the slight decrease of the melting temperature especially for the membranes with higher amount of GPTMS. This fact is due to the lower crystallization temperature in the cold crystallization peak in these samples that produce smaller crystals.

3.5. Water Sorption Measurements

Figure 5a shows the equilibrium water sorption isotherms up to water activity, α_w, of 0.95 at 25 °C for pure PLA,

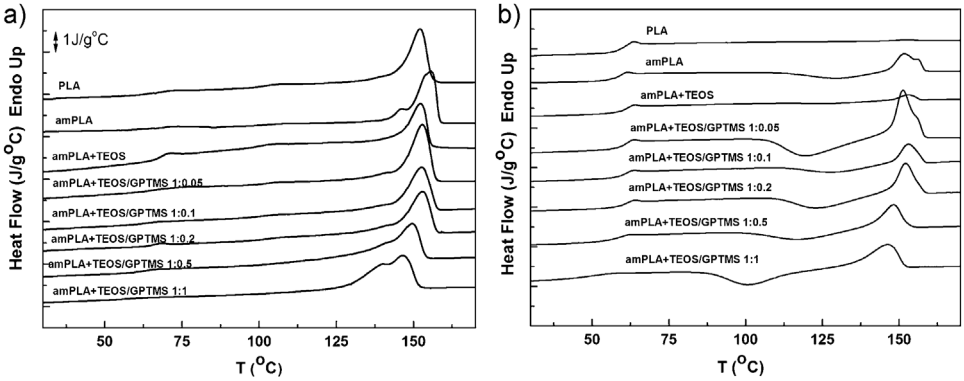

Figure 4. DSC thermograms recorded during first (a) and second (b) heating scan.

Table 3. Data extracted from the DSC thermogramsam regarding the first and second heating scan.

	First heat					Second heat					
sample	T_g [°C]	ΔC_p^* [J g^{-1} °C^{-1}]	T_m [°C]	ΔH [J g^{-1}]	x_c [%]	T_g [°C]	ΔC_p^* [J g^{-1} °C^{-1}]	T_{cc} [°C]	T_m [°C]	ΔH [J g^{-1}]	x_c [%]
PLA	63	0.10	155	22.0	23.7	60.0	0.6	–	152	0.3	0.0
amPLA	61	0.11	156	32.0	34.4	58.5	0.6	129.3	152 (157)	1.3	1.4
amPLA-TEOS	69	0.48	152	13.0	20.3	60.8	0.6	–	153	1.6	2.5
amPLA + TEOS/GPTMS 1:0.05	67	0.12	153	16.0	20.2	60.1	0.5	119.7	151 (156)	3.0	3.8
amPLA + TEOS/GPTMS 1:0.1	63	0.15	152	17.0	21.5	58.1	0.4	128.0	153	0.0	0.0
amPLA + TEOS/GPTMS 1:0.2	65	0.12	153	20.0	25.0	59.9	0.4	123.3	152	1.0	1.3
amPLA + TEOS/GPTMS 1:0.5	63	0.14	150	22.0	28.5	60.3	0.3	116.7	148	5.7	7.4
amPLA + TEOS/GPTMS 1:1	55	0.10	139 (147)	25.0	33.2	48.5	0.4	100.7	146	1.7	2.3

amPLA + TEOS/GPTMS 1:0.05, amPLA + TEOS/GPTMS 1:0.5 as well as for bulk TEOS/GPTMS 1:0.05 and TEOS/GPTMS 1:0.5. Firstly, the hydrophobic character of pure PLA is confirmed as the weight increase due to water adsorption reaches only 0.9% for the highest water activity. It should be kept in mind that PLA is in the glassy state at room temperature. An almost linear increase of wt% versus α_w is obtained with a slight upturn for the higher water activities. On the contrary, the equilibrium sorption isotherm of bulk TEOS/GPTMS 1:0.05 presents a different behavior with a high increase of water increase at low α_w followed by a linear increase for higher α_w. The above behavior is characteristic of a Type I in the Brunauer classification.[36] Type I also referred as Langmuir type sorption isotherms are characterized by their approach to a limiting value of adsorption, and usually describe adsorption onto microporous adsorbents in form of a monolayer, with strong sorbent–substrate interaction. The bulk sample obtained from TEOS/GPTMS 1:0.5 also present a distinct behavior that could be categorized in the Type III in the Brunauer classification. This class of isotherms describes adsorption onto adsorbents with weak adsorbate–adsorbent interactions. As seen on Figure 5a, an initial linear region for water activity up to 0.6 is observed, followed by a departure from linear behavior for $\alpha_w > 0.6$, which is typical for hydrogels and is explained in terms of clustering of water molecules. As concerns the hybrid membranes the sorption profile depends on the ratio of TEOS/GPTMS. From the above isotherms, it is clear that water sorption is greatly influenced by the characteristic sorption behavior of the

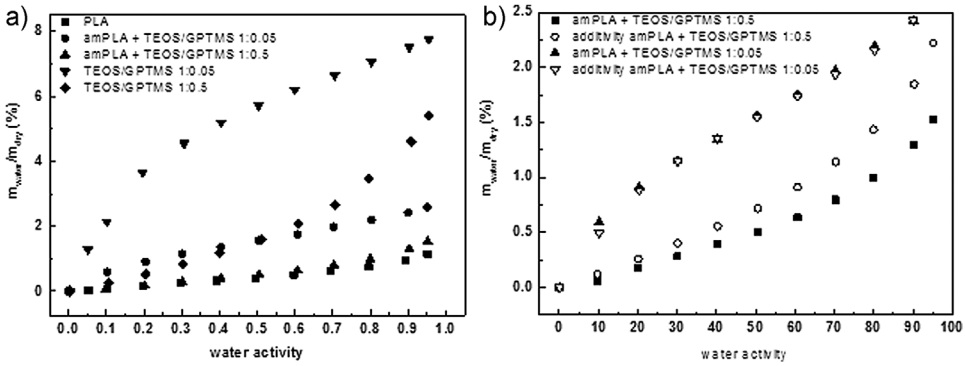

Figure 5. Equilibrium sorption isotherms of pure PLA and PLA + TEOS/GPTMS composites measured at room temperature.

Macromolecular Journals

Macromol. Biosci. **2014,** DOI: 10.1002/mabi.201400339

introduced inorganic phase of the hybrids. To further analyze the contribution of the inorganic phase by taking also into account the relative percentage in the final hybrid the Figure 5b is presented. In the latter, the measured sorption isotherms of the hybrids are given together with the theoretical isotherms calculated as a linear combination of the data for the pure components, that is, by assuming additivity. The curve corresponding to amPLA + TEOS/GPTMS 1:0.05 constructed using the additivity hypothesis coincides with the experimental sorption isotherm. The microporous nature of the absorbent, in this case the silica that covers the walls of the pores of PLA membranes, is clearly evidenced by the form of the sorption isotherm. On the contrary, the measured isotherm and the theoretical one assuming additivity of amPLA + TEOS/GPTMS 1:0.5 present different behavior. These isotherms correspond to absorbance by bulk polymers without indications of the presence of microporosity. Furthermore, a difference is observed when comparing the measured isotherm with the theoretical one with a lower water uptake observed for the former. This implies that fewer water adsorption sites are present after the introduction of TEOS/GPTMS compared to the hypothetical case that the two components would adsorb water independently. The above behavior could be attributed to the higher affinity of the reinforcement to the PLA thus providing an indirect indication of the interaction between the introduced phase and PLA.

3.6. Mechanical Properties

The mechanical properties of the membranes were studied by dynamic mechanical analysis. The steps appeared in the graphs of the dynamic storage modulus (E') in Figure 6a and the peaks in the graphs of tangent delta (tan δ) in Figure 6b correspond to the glass transition of PLA. A slight increase of the glass transition temperature is observed for the PLA + TEOS and for the amPLA + TEOS/GPTMS 1:0.05 in accordance with the DSC results obtained during the first heating scan. On the contrary, a slight decrease of T_g is observed for the hybrid membranes with higher GPTMS content. Furthermore, the elastic modulus of the hybrid composites also depends on the TEOS/GPTMS ratio in both, the glassy and the rubber-like state of the polymer. Thus, tuning the TEOS/GPTMS ratio we may modulate the mechanical response of the material. More specifically, an increase of E' in the glassy and rubbery state of the hybrids, as compared to neat PLA, is observed, except for the composite with TEOS/GPTMS 1:1. We recall, that a decrease of glass transition temperature T_g for the composites with the highest TEOS/GPTMS ratio (1:1) has been observed, while an increase of T_g for the composites with only TEOS and TEOS/GPTMS 0.05 has been observed. Therefore, our results may suggest that the TEOS/GPTMS ratio of 1:0.5 can lead to the optimum composition for improving the mechanical properties of the sample without altering the T_g. Interestingly, the main relaxation process of PLA broadens with the addition of the coating when it contains GPTMS what means that their organic side groups penetrate in the PLA walls deep enough to modify the conformational motions of PLA chains.

3.7. Osteogenic Differentiation Study

MSCs were seeded upon support materials in a two-dimensional monolayer culture at a density of 10 000 cells per sample. DNA content of attached mesenchymal stem cells was determined with Picrogreen® assay. As can be seen in Table 4, all the samples showed a similar cell seeding efficiency and proliferate through the time except for amPLA + TEOS:GPTMS 1:0.05 sample, which showed the lowest DNA content and did not show cell proliferation (Figure 7).

There was a concern that the direct contact of the cells with unreacted epoxy groups exhibited at the surface of the supports could have a cytotoxic effect due to the reaction of these reactive groups with amine groups in proteins of cell membranes. Indirect cytotoxicity studies (ISO 10993-5)

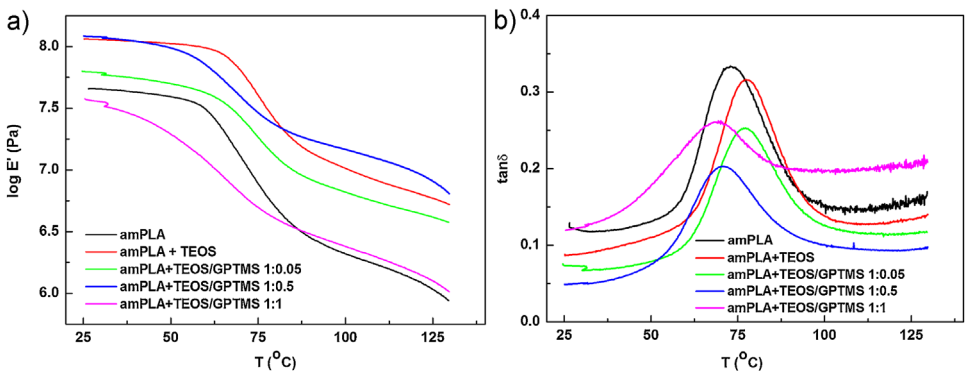

Figure 6. Storage modulus (a) and tan δ (b) for amPLA and amPLA + TEOS/GPTMS hybrids obtained by DMA.

Table 4. Percentage of seeding efficiency calculated as ((ng $DNA_{sample,1d} \times$ ng DNA $_{cell}$)/density of seeding) $\times$ 100, for all materials.

Sample	Seeding efficiency [%]
PLA	41.30 ± 5.64
amPLA	40.46 ± 9.50
amPLA + TEOS	34.67 ± 9.72
amPLA + TEOS:GPTMS 1:0.05	46.14 ± 18.20
Control	31.38 ± 1.76

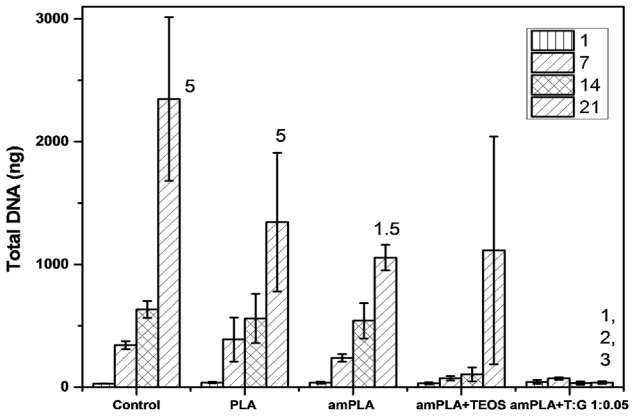

Figure 7. Quantification of total DNA at 1, 7, 14, and 21 d for different materials. Significance of p-value < 0.05 compared to similar group is signaled as 1 (Control), 2 (PLA), 3 (amPLA), 4 (amPLA + TEOS), 5 (amPLA + TEOS:GPTMS 1:0.05) for each group at the same time.

were performed previously in films of polysaccharide containing GPTMS and TEOS.[37] Briefly, different films with various GPTMS:TEOS molar ratios were studied immersing them in culture media for 24 h. This culture media with the by-products of the materials was used to feed a 24 h fibroblast L292 culture in a 96-well-multiplate. After 24 h, the viability of cells was tested by means of MTT assay. The results showed that the presence of GPTMS did not show any cytotoxic effect, therefore, it was concluded that GPTMS do not liberate any toxic by-product.[37] The above findings are also supported by studies on hybrid materials incorporating GPTMS, which exhibited excellent levels of cytocompatibility with human MG63 osteosarcoma cells, and human bone marrow osteoblasts.[38,39] However, in spite that cell numbers on amPLA + TEOS:GPTMS supports are much smaller than in PLA or amPLA + TEOS supports, osteoblastic differentiation of MSCs on GPTMS containing supports is significantly improved with respect to pure PLA supports.

PLA TEOS membranes had a proliferation profile smaller than PLA membranes but higher than GPTMS containing membranes.

Osteogenic differentiation was evaluated by collagen quantification, determination of alkaline phosphatase activity and histochemistry. Collagen content was determined by the oxidation of hydroxyproline, which is an imino acid typical of collagen. Briefly, the hydroxyproline contains a pyrrolidine ring that can oxidize into a pyrrole ring, which can be determined by a reaction using Ehrlich's reagent, resulting in a quinoid compound that is colored. The quantification of collagen via hydroxylation of hydroxyproline is shown in Figure 8a. As expected, the major amount of collagen was at 21 d in all materials, when cells have been deposited the extracellular matrix. It is interesting to note that in amPLA + TEOS membranes the production of collagen starts at 7 d with the highest amount of collagen. Collagen normalized respect to DNA content (Figure 8b) showed similar values for all non-hybrid samples. Hybrid materials showed the highest normalized collagen content pointing to cells with more synthetic capacity compared to cells seeded on naked materials.

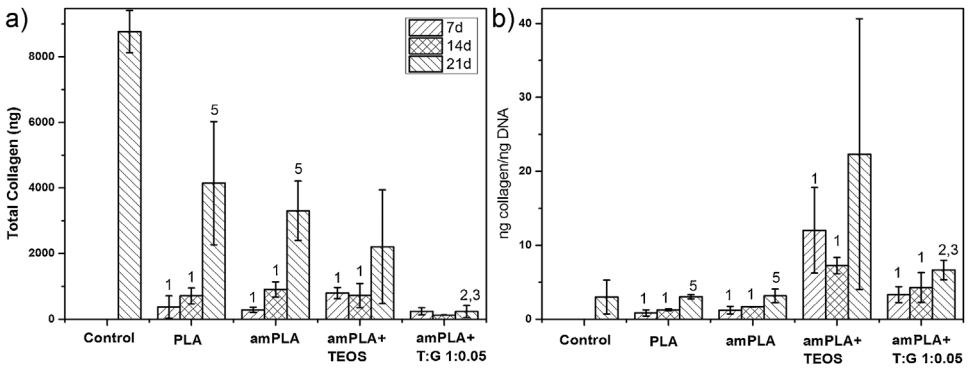

Figure 8. a) Quantification of collagen by means of hydroxylation of hydroxyproline for three different times (7, 14, and 21 d) in different materials; b) representation of the collagen normalized respect to DNA in each sample. Significance of p-value < 0.05 compared to similar group is signaled as 1 (Control), 2 (PLA), 3 (amPLA), 4 (amPLA + TEOS), 5 (amPLA + TEOS:GPTMS 1:0.05) for each group at the same time.

Macromolecular Journals

Macromol. Biosci. **2014,** DOI: 10.1002/mabi.201400339

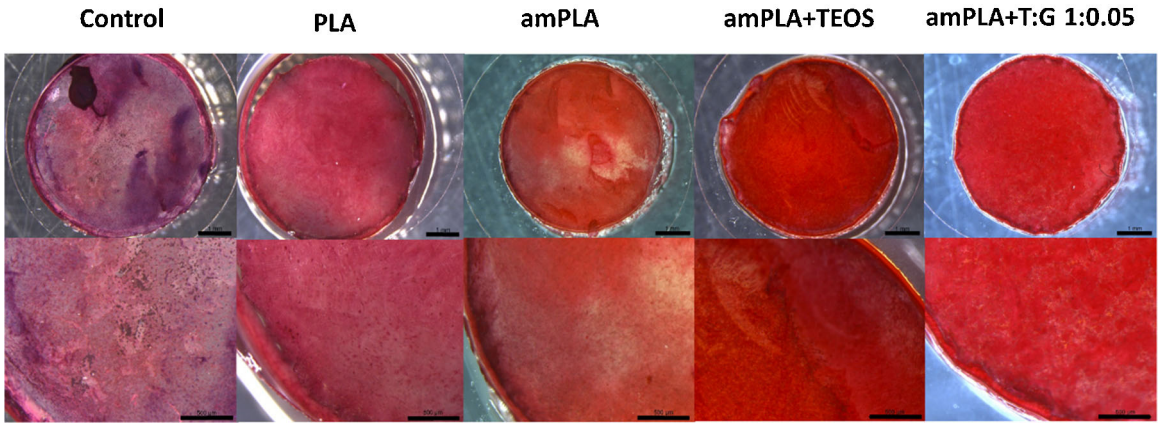

Figure 9. Picrosirius red staining of 21 d cell seeded materials. Scale bar for the upper picture of each material: 1 mm and scale bar for the lower picture of each material: 500 μm.

Histological staining for collagen was performed with picrosirius red. Sirius red molecule binds to triple helical collagen and does not bind to degraded collagen or other proteins without the typical triple helical conformation of collagen. Figure 9 shows the images taken with a stereoscopic microscope for the picrosirius red staining, the blank was performed with each material stained in their acellular form. The typical red-orange staining was seen for amPLA and hybrid membranes showing amPLA + TEOS the most intense stain. The control did not show presence of collagen staining. It is worth noting the intense coloration of amPLA + TEOS:GPTMS support in spite to the small number of cells.

Calcium phosphate is the most abundant mineral compound on bone extracellular matrix. The presence of calcium was detected through alizarin red staining (Figure 10). Alizarin red S is an anthraquinone derivative, which binds to calcium in a chelation process. Figure 10 shows the pictures taken for the calcium staining. In general, there is no presence of calcium aggregates except for amPLA + TEOS:GPTMS 1:0.05 material, which have small calcium–alizarin red S complexes.

When MSCs are cultured in presence of ascorbic acid, β-glycerol phosphate, and dexamethasone acquire osteoblastic like phenotype with upregulated alkaline phosphatase activity. Therefore, ALP activity was used as a biochemical marker for the osteoblast phenotype and it is presented in Figure 11. amPLA showed the major ALP activity in terms of total product, however GPTMS hybrid membrane present the major normalized ALP activity respect to DNA.

The above results for the evaluation of the osteogenic differentiation, PLA, amPLA, and amPLA + TEOS samples did not show significant differences with respect to the expression of osteogenic markers although amPLA + TEOS show a significantly higher production of extracellular matrix.

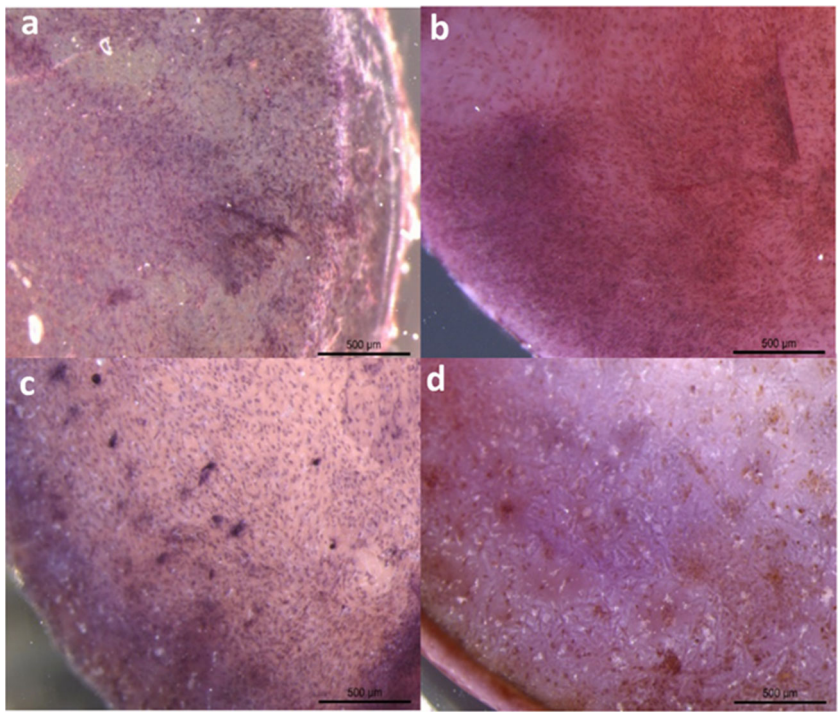

Figure 10. Alizarin RedS staining of 21 d cell seeded materials. a) Control, b) PLA, c) amPLA + TEOS, and d) amPLA + TEOS:GPTMS 1:0.05. Scale bar: 500 μm.

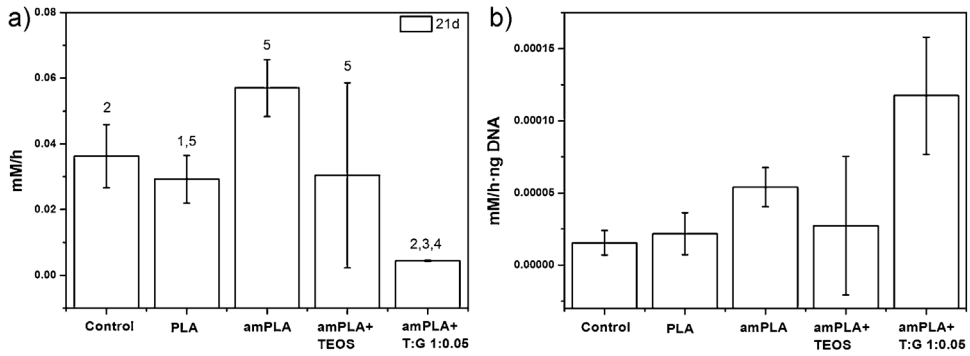

Figure 11. a) Quantification of the ALP activity at 21 d showed as mM *p*-nitrophenol per hour, b) representation of the ALP activity normalized to DNA. Significance of *p*-value <0.05 compared to similar group is signaled as 1 (Control), 2 (PLA), 3 (amPLA), 4 (amPLA + TEOS), 5 (amPLA + TEOS:GPTMS 1:0.05) for each group at the same time.

GPTMS-coated membranes, which form a very complex network, seem to produce cell death as can be observed at the Figure 7. Nevertheless, it has been shown that the GPTMS-containing membrane present the highest osteoblastic-like phenotype showing high levels of normalized collagen content respect DNA, high collagen staining, some calcium staining, and the highest levels of normalized ALP activity respect DNA. Nevertheless, inactivation of unreacted epoxy groups seems to be a requirement and the follow up of the cytotoxicity of the degradation products during silica network dissolution in biological fluids is necessary.

4. Conclusion

Hybrid porous membranes were obtained following a novel strategy for the reinforcement of already prepared porous polymer membranes with silica. Firstly, porous PLA membranes were prepared using freeze extraction techniques. Pore walls were functionalized by an aminolysis treatment to introduce amine groups in their surfaces. In a second stage, silica phase was produced by sol–gel reactions inside the pores using TEOS and GPTMS as the silica precursors and HCL as the acid catalyzer. GPTMS served also as a coupling agent between the organic phase and the silica network. The molar ratio of GPTMS with respect to TEOS in the sol–gel solution was varied between 0.05 and 1. FTIR study revealed the successful introduction of amino groups on PLA surface and provided indications of the bonding with silica phase through GPTMS. SEM showed that the inorganic silica phase forms a co-continuous phase with the polymer phase and that the porous architecture is retained. Furthermore, the coupling between polymer phase and GPTMS was probed by significant changes in segmental dynamics of amorphous phase of PLA as revealed in DSC and dynamic-mechanical experiments. The elastic modulus of the hybrid composites depends on the TEOS/GPTMS ratio both in the glassy and the rubber-like states of the polymer what allows modulating the mechanical response of the material. The shape of the equilibrium sorption isotherms from water vapor sorption measurements provided valuable information regarding the structure of the silica coating of the PLA pores with respect to GPTMS content and supports the hypothesis of the coupling between the inorganic and polymer phase. On the other hand, mesenchymal stem cell in vitro studies were performed showing a scarce initial adhesion in GPTMS containing membranes, however, the few cells attached to the membrane showed the highest osteoblastic-like phenotype in the differentiation study as shows the collagen and ALP activity quantification and also the staining performed.

The presented method of preparation could be applied for the fabrication of macroporous hybrid scaffolds for tissue engineering and extended to incorporate bioactive glass providing thus tailorable ion release for bone bonding applications. Furthermore, the potential use of the obtained porous hybrid structures is not limited to porous membranes for tissue engineering approaches. The proposed strategy is applicable for the preparation of hybrids using various polymers and combined with the great versatility of the sol–gel method through the adjustment of the reaction parameters and the precursors ratio, could allow the modification of the final porosity to meet the specific needs of applications such as ultrafiltration or pervaporation.

Acknowledgements: The research project is implemented within the framework of the Action "Supporting Postdoctoral Researchers" of the Operational Program "Education and Lifelong Learning" (Action's Beneficiary: General Secretariat for Research and Technology), and is co-financed by the European Social Fund (ESF) and the Greek State, Grant No.: NARGEL-PE5(2551). J.R.R. acknowledges funding of his PhD by the Generalitat Valenciana through VALi+d grant (ACIF/2010/238). J.F.M. thanks the Portuguese Foundation for Science and Technology (FCT) for financial

support through the PTDC/FIS/115048/2009 project. J.L.G.R. acknowledges the support of the Ministerio de Economía y Competitividad, MINECO, through theMAT2013-46467-C4-1-R project. CIBER-BBN is an initiative funded by the VI National R&D&I Plan 2008-2011, Iniciativa Ingenio 2010, Consolider Program, CIBER Actions and financed by the Instituto de Salud Carlos III with the assistance from the European Regional Development Fund.

Received: July 22, 2014; Revised: September 10, 2014; Published online:DOI: 10.1002/mabi.201400339

Keywords: organic–inorganic hybrid composites; porosity; proliferation and osteoblastic differentiation of cells; sol–gel processes; thermomechanical properties

[1] A. Södergård, M. Stolt, "Industrial Production of High Molecular Weight Poly(Lactic Acid)", in *Poly(Lactic Acid): Synthesis, Structures, Properties, Processing, and Applications* (Eds: L.-T. L. R. Auras, S. E. M. Selke, H. Tsuji), John Wiley & Sons, Inc., Hoboken, NJ, USA **2010**, p. 27.
[2] K. Madhavan Nampoothiri, N. R. Nair, R. P. John, *Bioresource Technol.* **2010**, *101*, 8493.
[3] I. Izal, P. Aranda, P. Sanz-Ramos, P. Ripalda, G. Mora, F. Granero-Moltó, H. Deplaine, J. L. Gómez-Ribelles, G. G. Ferrer, V. Acosta, I. Ochoa, J. M. García-Aznar, E. J. Andreu, M. Monleón-Pradas, M. Doblaré, F. Prósper, *Knee Surg., Sports Traumatol., Arthrosc.* **2013**, *21*, 1737.
[4] R. A. Jain, *Biomaterials* **2000**, *21*, 2475.
[5] J. Yan-Peng, C. Fu-Zhai, *Biomed. Mater.* **2007**, *2*, R24.
[6] Y. Zhu, Z. Mao, C. Gao, *RSC Adv.* **2013**, *3*, 2509.
[7] L. Yu, K. Dean, L. Li, *Prog. Polym. Sci. (Oxford)* **2006**, *31*, 576.
[8] K. Rezwan, Q. Z. Chen, J. J. Blaker, A. R. Boccaccini, *Biomaterials* **2006**, *27*, 3413.
[9] G. Wei, P. X. Ma, *Biomaterials* **2004**, *25*, 4749.
[10] S. S. Ray, K. Yamada, M. Okamoto, K. Ueda, *Nano Lett.* **2002**, *2*, 1093.
[11] C.-S. Wu, H.-T. Liao, *Polymer* **2007**, *48*, 4449.
[12] S. Verrier, J. J. Blaker, V. Maquet, L. L. Hench, A. R. Boccaccini, *Biomaterials* **2004**, *25*, 3013.
[13] G. Z. Papageorgiou, D. S. Achilias, S. Nanaki, T. Beslikas, D. Bikiaris, *Thermochim. Acta* **2010**, *511*, 129.
[14] K. Fukushima, D. Tabuani, C. Abbate, M. Arena, P. Rizzarelli, *Eur. Polym. J.* **2011**, *47*, 139.
[15] B. Demirdögen, C. E. Plazas Bonilla, S. Trujillo, J. E. Perilla, A. E. Elcin, Y. M. Elcin, J. L. Gómez Ribelles, *J. Biomed. Mater. Res. A* **2014**, *102*, 3229.
[16] C. Pandis, S. Madeira, J. Matos, A. Kyritsis, J. F. Mano, J. L. G. Ribelles, *Mater. Sci. Eng. C* **2014**, *42*, 553.
[17] M. H. Ho, P. Y. Kuo, H. J. Hsieh, T. Y. Hsien, L. T. Hou, J. Y. Lai, D. M. Wang, *Biomaterials* **2004**, *25*, 129.
[18] Y. Gong, Y. Zhu, Y. Liu, Z. Ma, C. Gao, J. Shen, *Acta Biomater.* **2007**, *3*, 677.
[19] P. C. Painter, M. M. Coleman, *Fundamentals of Polymer Science: An Introductory Text*, 2nd Edition Technomic Publishing Co., Lancaster **1997**.
[20] L. Liu, M. L. Fishman, K. B. Hicks, C. K. Liu, *J. Agric. Food Chem.* **2005**, *53*, 9017.
[21] L. A. Gaona, J. L. Gómez Ribelles, J. E. Perilla, M. Lebourg, *Polym. Degrad. Stabil.* **2012**, *97*, 1621.
[22] N. Y. Ignat'eva, N. A. Danilov, S. V. Averkiev, M. V. Obrezkova, V. V. Lunin, E. N. Sobol, *J. Anal. Chem.* **2007**, *62*, 51.
[23] W. E. Kafienah, T. J. Sims, in *Biopolymer Methods in Tissue Engineering*, Eds., A. P. Hollander, P. V. Hatton), Humana Press, Totowa, NJ **2004**, p. 217.
[24] Y. Zhu, C. Gao, X. Liu, T. He, J. Shen, *Tissue Eng.* **2004**, *10*, 53.
[25] G. Kister, G. Cassanas, M. Vert, *Polymer* **1998**, *39*, 267.
[26] D. Garlotta, *J. Polym. Environ.* **2001**, *9*, 63.
[27] F. Causa, E. Battista, R. Della Moglie, D. Guarnieri, M. Iannone, P. A. Netti, *Langmuir* **2010**, *26*, 9875.
[28] S. Yuan, G. Xiong, A. Roguin, C. Choong, *Biointerphases* **2012**, *7*, 30.
[29] V. A. Santamaría, H. Deplaine, D. Mariggió, A. R. Villanueva-Molines, J. M. García-Aznar, J. L. G. Ribelles, M. Doblaré, G. G. Ferrer, I. Ochoa, *J. Non-Crystal. Solids* **2012**, *358*, 3141.
[30] W. Stöber, A. Fink, E. Bohn, *J. Colloid Interface Sci.* **1968**, *26*, 62.
[31] L. L. Hench, J. K. West, *Chem. Rev.* **1990**, *90*, 33.
[32] C. Pandis, A. Spanoudaki, A. Kyritsis, P. Pissis, J. C. R. Hernández, J. L. Gómez Ribelles, M. Monleón Pradas, *J. Polym. Sci. B: Polym. Phys.* **2011**, *49*, 657.
[33] F. Carrasco, P. Pagès, J. Gámez-Pérez, O. O. Santana, M. L. Maspoch, *Polym. Degrad. Stabil.* **2010**, *95*, 116.
[34] J. F. Mano, J. L. Gómez Ribelles, N. M. Alves, M. Salmerón Sanchez, *Polymer* **2005**, *46*, 8258.
[35] Y. Wang, J. L. Gómez Ribelles, M. Salmerón Sánchez, J. F. Mano, *Macromolecules* **2005**, *38*, 4712.
[36] S. Brunauer, L. S. Deming, W. E. Deming, E. Teller, *J. Am. Chem. Soc.* **1940**, *62*, 1723.
[37] E. Pérez-Román, *Bachelor Thesis*, Universitat Politècnica de València, **2014**.
[38] Y. Shirosaki, K. Tsuru, S. Hayakawa, A. Osaka, M. A. Lopes, J. D. Santos, M. H. Fernandes, *Biomaterials* **2005**, *26*, 485.
[39] Y. Shirosaki, M. Hirai, S. Hayakawa, E. Fujii, M. A. Lopes, J. D. Santos, A. Osaka, *J. Biomed. Mater. Res. A* **2014**, in press, DOI: 10.1002/jbm.a.35171.